

Full Paper

Cantilever measurements of surface stress, surface reconstruction, film stress and magnetoelastic stress of monolayers

Dirk Sander^{1,*}, Zhen Tian¹ and Jürgen Kirschner¹

¹Max-Planck-Institut für Mikrostrukturphysik, Weinberg 2, D-06120 Halle, Germany

E-mail: (sander@mpi-halle.de).

* Author to whom correspondence should be addressed.

Received: 4 March 2008; in revised form: 16 May 2008 / Accepted: 16 May 2008 / Published: 29 July 2008

Abstract: We review the application of cantilever-based stress measurements in surface science and magnetism. The application of thin (thickness appr. 0.1 mm) single crystalline substrates as cantilevers has been used successfully to measure adsorbate-induced surface stress changes, lattice misfit induced film stress, and magneto-elastic stress of ferromagnetic monolayers. Surface stress changes as small as 0.01 N/m can be readily measured, and this translates into a sensitivity for adsorbate-coverage well below 0.01 of one layer. Stress as large as several GPa, beyond the elasticity limits of high strength materials, is measured, and it is ascribed to the lattice misfit between film and substrate. Our results point at the intimate relation between surface stress and surface reconstruction, stress-induced structural changes in epitaxially strained films, and strain-induced modifications of the magneto-elastic coupling in ferromagnetic monolayers.

Keywords: cantilever stress measurement, surface stress, surface reconstruction, film stress, magnetoelastic stress, torque magnetometry.

1 Introduction

The stress-induced curvature of thin substrates offers an appealing way to deduce stress at surfaces and in thin films directly. Cantilever substrates, i.e. thin substrates, which are clamped along the width to a sample manipulator, where the substrate remains free to bend along its length, have been employed

successfully in numerous stress studies. Highly sensitive and accurate quantitative data on stress in films and at surfaces have been obtained. Several reviews and articles present results on adsorbate-induced surface stress, film stress, and magnetoelastic stress [1–19].

In addition to these stress measurements, also the mechanical torque between an external magnetic field and the total magnetic moment of a sample has been exploited successfully in cantilever experiments to perform quantitative torque magnetometry on films as thin as a few atomic layers [20–23]. The aspect of torque magnetometry is treated in another contribution to this cantilever issue of *Sensors*.

We start with a discussion of experimental aspects regarding cantilever-based stress measurements, where we address cantilever clamping and elastic anisotropy. Both aspects need to be considered to ensure a proper quantitative analysis of the stress-curvature relations, which are the basis of cantilever measurements. Then, we present examples of cantilever experiments which we performed to study the role of stress at surfaces and in ultrathin epitaxial films for surface reconstruction, surface alloying, structural transitions and the magnetoelastic coupling in strained ferromagnetic layers.

2 Experimental Section

In contrast to the seemingly simple experimental scheme of a cantilever stress measurements, there are two subtle caveats, which need to be considered to ensure a proper data analysis. Firstly, we comment on how the clamping of the cantilever needs to be considered to ensure a straightforward data analysis. Secondly, we illustrate how the anisotropy of the elastic properties enters the data evaluation. Before we discuss how both aspect are treated in the curvature analysis, we briefly introduce the venerable *Stoney equation*, which gives the relation between substrate curvature and stress.

Some 100 years ago Stoney has exploited the stress-induced curvature of a thin ruler, which served as a substrate to investigate the stress of an electroplated Ni film [24]. He gave the relation between film stress τ , film thickness t and curvature $1/R$ as $\tau t = Y t_s^2 / (6R)$, where Y : Young modulus of the substrate, and t_s : thickness of the substrate.

Ever since a relation between stress τ and curvature $1/R$ has been described as *Stoney equation*. This is cumbersome, as the original *Stoney equation* given above is not valid in general, as it describes a one-dimensional stress-curvature scenario. This is not fulfilled in most applications. Rather, the film is under a biaxial stress. It has been indicated before [8] that under biaxial stress, the substrate stiffness should enter in the form $Y/(1 - \nu)$, with ν : Poisson ratio, and not in the form Y , as given above. This leads to a sizeable correction for the calculation of stress due to the magnitude of $\nu \approx 0.4$. Values of the Young modulus and the Poisson ratio are given in Table 1 below for some elements.

2.1 The role of cantilever clamping and elastic anisotropy for quantitative analyses

An important aspect for the proper quantitative analysis of cantilever measurements is the influence of cantilever clamping onto the biaxial stress-induced curvature. In most cases the cantilever is clamped along its width at its upper end, as schematically shown in Fig. 1. This clamping has an important influence on the stress-induced curvature of the cantilever, as it hinders a free two-dimensional curvature. The curvature along the width of the cantilever is suppressed near the clamping. Further away from the clamping, a cantilever curvature along the width is possible. Thus, one expects a transition from 1-dimensional to 2-dimensional curvature with increasing length-to-width ratio of the cantilever.

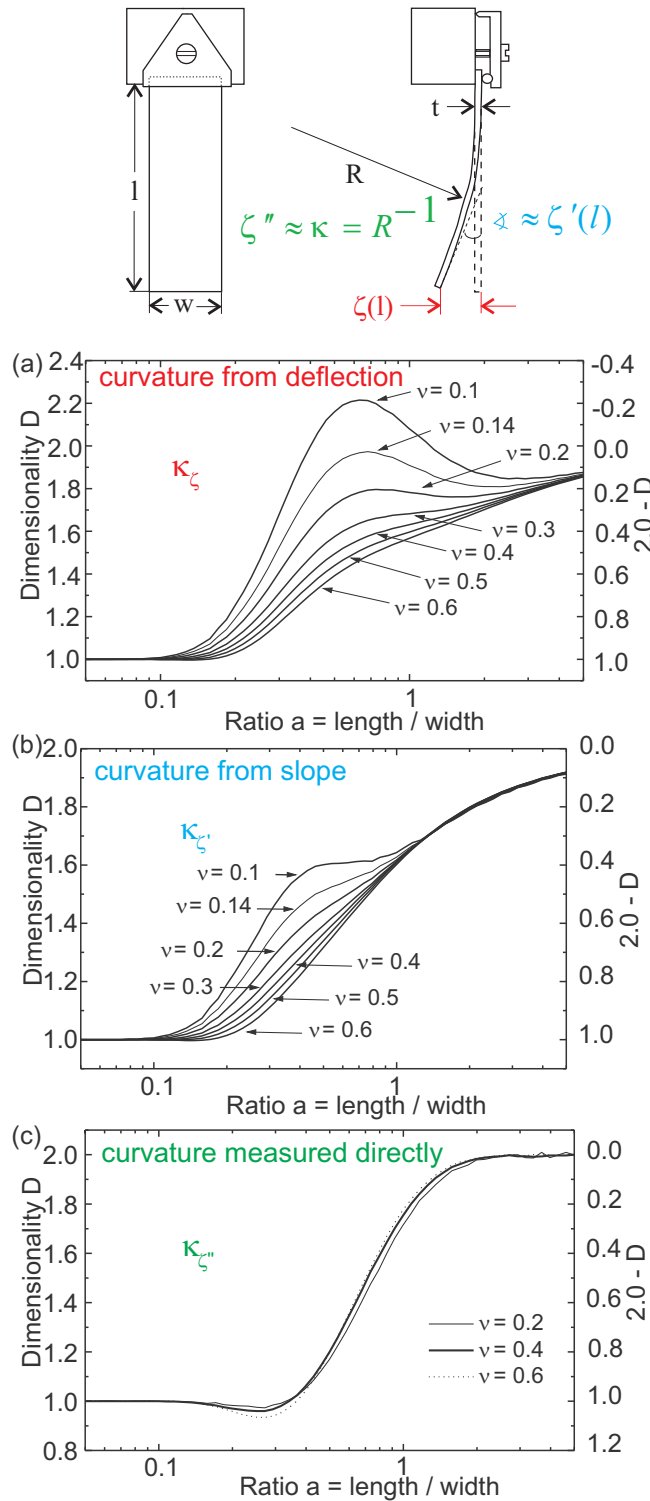


Figure 1. Deflection ξ , slope ξ' , and curvature ξ'' of a curved cantilever of length l and width w . Plots (a), (b), and (c) give the dimensionality D , derived from finite element calculations [25] for an isotropic substrate under isotropic biaxial stress for deflection, slope and curvature measurements, respectively. A direct curvature measurement is preferable, as it requires the smallest corrections for length-to-width ratios larger than two. The different plots within each panel indicate the dependence of D on the magnitude of the Poisson ratio ν .

Thorough finite element analyses [25] corroborate this assertion. Careful studies provide a quantitative description of the relation between the dimensionality of the curvature and the length-to-width ratio and the Poisson ratio of the cantilever substrate. The results of the finite element analysis are summarized in Fig. 1.

These calculations clearly reveal that the corrections in the data analysis depend on whether a measurement of the cantilever deflection, slope or curvature is performed. The calculations indicate that a direct curvature measurement is preferable as it suffers the least from the adverse effect of clamping. Here, a 2-dimensional curvature resembles a very good approximation already for a length-to-width ratio larger than two, whereas sizeable corrections are compulsory for the quantitative analysis based on deflection and slope measurements [25].

An optical two-beam deflection technique offers a venue towards direct curvature measurements, and it will be described below. The *generalized Stoney equation*, see eq. 1, has been introduced to address the issue of dimensionality D of curvature properly as

$$\text{generalized Stoney equation : } \tau t = \frac{Y t_s^2}{6(1-\nu)(1+(2-D)\nu)} \frac{1}{R} \quad (1)$$

$$1 - \text{dimensional curvature : } \tau t = \frac{Y t_s^2}{6(1-\nu^2)} \frac{1}{R} \quad (2)$$

$$2 - \text{dimensional curvature : } \tau t = \frac{Y t_s^2}{6(1-\nu)} \frac{1}{R}, \quad (3)$$

where the limiting cases of 1-dimensional and 2-dimensional curvature are obtained for $D = 1$ and $D = 2$, respectively. These equations are valid for elastically isotropic substrates under the influence of isotropic stress, and therefore the tensor character of τ could be safely disregarded.

Note, however, that only for an isotropic stress $\tau = \tau_x = \tau_y$, a measurement of a single curvature $1/R$ suffices to give the stress τ . In the more general case of anisotropic stress, two radii of curvature $1/R_x$, $1/R_y$ need to be measured to obtain the stress components τ_x and τ_y , where x , y indicate two orthogonal directions in the cantilever plane [8]:

$$\tau_x t = \frac{Y t_s^2}{6(1-\nu^2)} \left(\frac{1}{R_x} + \nu \frac{1}{R_y} \right) \quad (4)$$

$$\tau_y t = \frac{Y t_s^2}{6(1-\nu^2)} \left(\frac{1}{R_y} + \nu \frac{1}{R_x} \right). \quad (5)$$

In cases where the two radii of curvature cannot be extracted from one measurement, one needs to perform measurements on two differently cut cantilevers, where the lengths are either along the x - or the y -direction. Such measurements have been performed e.g. to extract the anisotropic film stress for Fe and Ni monolayers on W(110) [8, 14, 26], and the anisotropic surface stress change upon oxygen adsorption on W(110), which induces an anticlastic curvature of the W substrate [26].

2.2 The role of elastic anisotropy for quantitative analyses

The use of crystalline substrates requires to consider the directional dependence of the elastic properties, as they are anisotropic in general. This elastic anisotropy can be sizeable.

Table 1. Selected elastic compliances s_{ij} in TPa^{-1} [28–30], also for elements treated in Fig. 2. The Young modulus Y in GPa, the Poisson ratio ν , and the biaxial modulus $Y/(1-\nu)$ in GPa are given for a $\langle 100 \rangle$ direction.

	s_{11}	s_{12}	s_{44}	Y	ν	$Y/(1-\nu)$
Si	7.73	-2.15	12.7	129	0.278	179
Cu	15.0	-6.3	13.2	67	0.420	115
W	2.45	-0.69	6.24	408	0.282	568
Ir	2.26	-0.67	3.8	442	0.296	629
MgO	4.01	-0.96	6.48	249	0.239	328
GaAs	11.73	-3.66	16.84	85	0.312	124

To illustrate the directional dependence of the elastic properties, we show in Fig. 2 polar plots of the Young modulus Y , where both polar 3d-plots and an azimuthal scan within the (111) plane are shown. The corresponding tensor transformation have been applied for the elastic compliances s_{11} , s_{12} , and s_{44} , which are connected to the Young modulus Y and the Poisson ratio ν for direction along the cubic axes as $Y = 1/s_{11}$ and $\nu = -s_{12}/s_{11}$, as given in detail in references [8, 27].

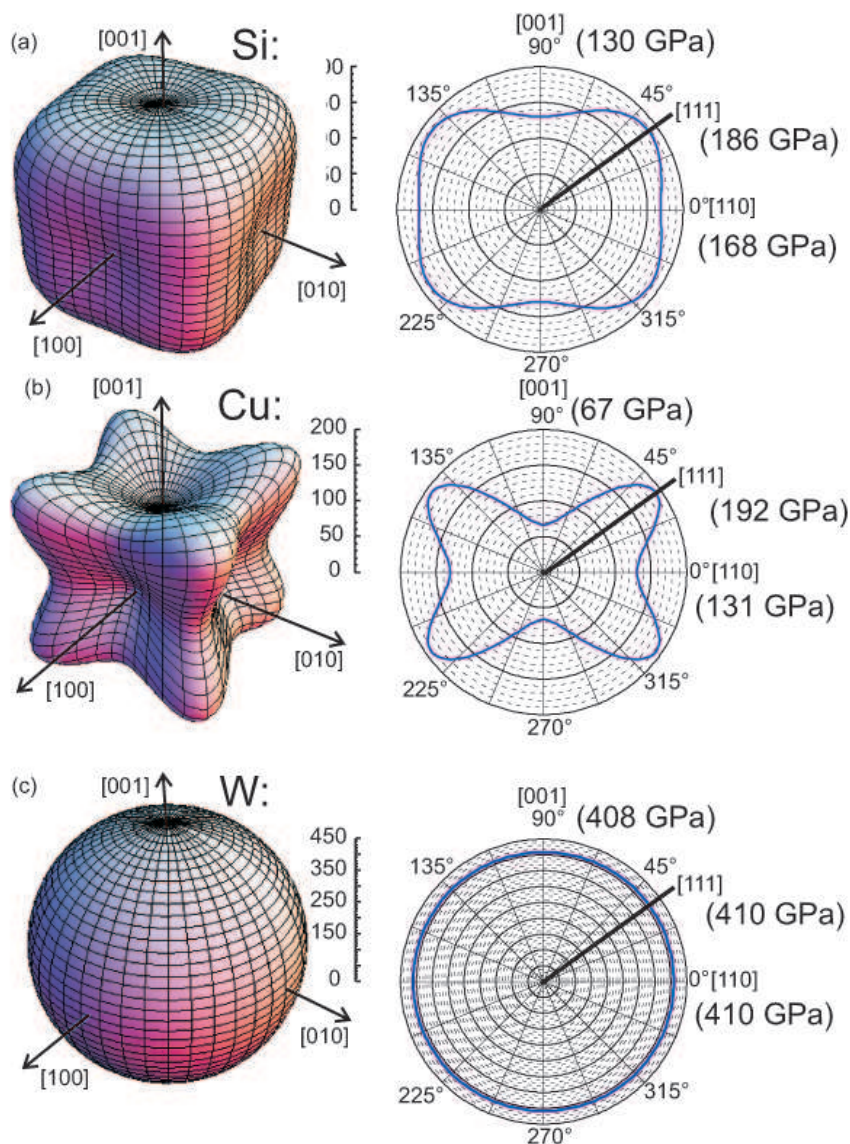


Figure 2. Directional dependence of the Young modulus Y of (a) Si, (b) Cu, and (c) W. The left panel gives 3d-polar plots of Y , the right panel shows the azimuthal variation of Y within the (111) plane. Y is given in parentheses for the [001], [111], and [110] direction. Note the almost isotropic behavior for W.

A pronounced anisotropy is obvious for Si and Cu. Here, Y is large along [111], small along [100], and intermediate along [110], as indicated by the values given in parentheses in Fig. 2(b). The magnitude and the direction of the extrema of Y depend on the specific element under consideration [8]. The Young modulus of W turns out to be almost isotropic, with a minute relative variation of ($\Delta Y/Y < 0.005$). This negligible anisotropy was exploited in the first 2-dimensional stress analysis cited above [8, 14, 26]. A constant value of the elastic properties of the substrate resembles a valid approximation for W.

For crystalline cantilevers, the elastic properties Y and ν need to be calculated for the chosen crystalline orientation. The required tensor transformations are described in detail in reference [8, 31].

The symmetry of the directional dependence of Y and ν leads to isotropic values for $Y/(1 - \nu)$ for directions within the (001) planes, whereas Y and ν are both isotropic within (111)-planes of cubic materials, and also within the basal plane (0001) of hexagonal materials [8, 31].

The following expressions give the expression for Y , ν , and the biaxial modulus $Y/(1 - \nu)$ for two common orientations in terms of the tabulated elastic compliances s_{ij} , which are to be used in the *Stoney equations* 1 given above.

$$(001) : Y = \frac{1}{s_{11}}, \nu = -\frac{s_{12}}{s_{11}}, \frac{Y}{1 - \nu} = \frac{1}{s_{11} + s_{12}} \quad (6)$$

$$(111) : Y = \frac{1}{s_{11} - \frac{1}{2}s}, \nu = -\frac{s_{12} + \frac{1}{6}s}{s_{11} - \frac{1}{2}s}, \frac{Y}{1 - \nu} = \frac{6}{4s_{11} + 8s_{12} + s_{44}} \quad (7)$$

$$\text{with } s = s_{11} - s_{12} - \frac{1}{2}s_{44}.$$

The magnitude of the expression $s = s_{11} - s_{12} - \frac{1}{2}s_{44}$ reflects the elastic anisotropy; s can be positive or negative, depending on the element. A value close to zero indicates negligible anisotropy, which is observed in very good approximation for W (W: $s = 0.02 \text{ TPa}^{-1}$).

For the cubic (110) orientation less simplification is possible. Here, two radii of curvature R_1 and R_2 need to be measured, and the proper tensor transformations need to be applied for s_{ij} [7, 8]. However, provided that the substrate shows isotropic elastic behavior, the relations cited above in eq. 4 give the proper relation between curvature and stress for the (110) orientation.

2.3 Optical curvature measurement under ultrahigh vacuum conditions and in magnetic fields

The discussion of the curvature-stress relation above and the plots of Fig. 1 clearly suggests that a direct measurement of the stress-induced curvature change of a thin substrate is advisable. This assertion is based on the understanding that a curvature measurement is affected the least, as compared to deflection and slope measurements, from the adverse effect of sample clamping on substrate curvature [25].

A simple, yet very powerful technique to measure a stress-induced curvature is the analysis of the deflection of laser beams upon reflection from a curved substrate surface. A schematic and the realization of the optical curvature measurement are shown in Fig. 3.

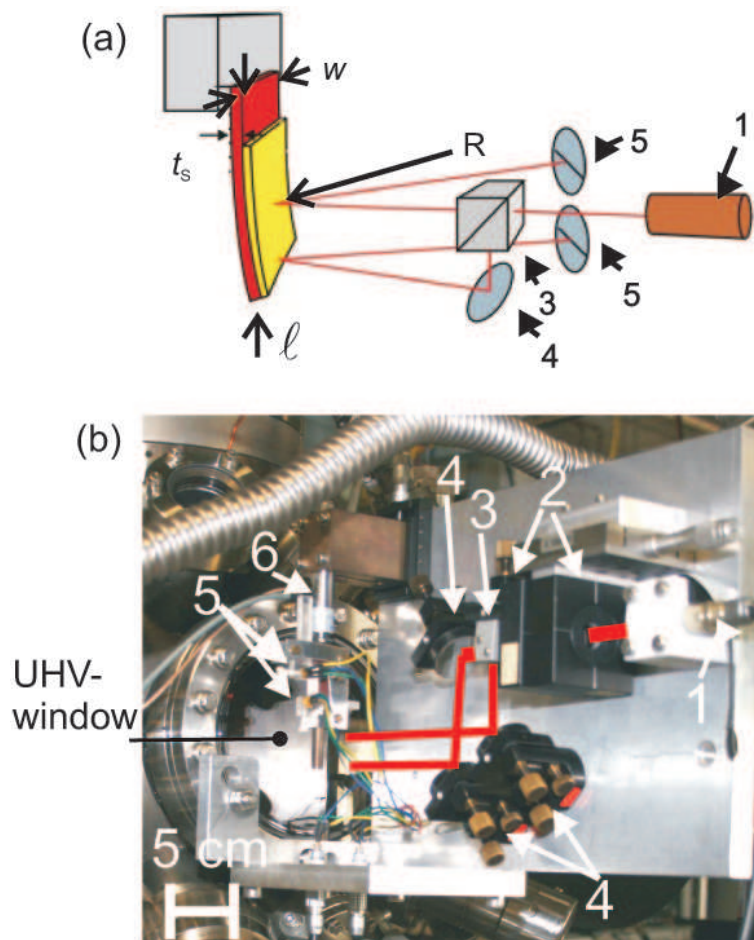


Figure 3. Optical two beam deflection technique. (a) Sketch of the set-up. The substrate of length ℓ , width w , and thickness t_s is fixed along its width at the top end. The curvature $1/R$ of the substrate is monitored by reflecting two laser beams onto position sensitive detectors. (b) Set-up mounted to a window flange of an UHV chamber, the substrate is located inside of the chamber, behind the window. 1: laser, 2: lenses for beam focusing, 3: beam splitter, 4: mirrors, 5: position sensitive detector (split-photodiode).

One main advantage of the optical deflection technique is that only a thin cantilever substrate with optical access to the sample surface for incoming and reflected beams is needed. Commercial multiple optical beam deflection measurements are available [32].

All results presented here were obtained with our home-built set up, shown in Fig. 3, which has been used successfully to measure minute surface stress changes during adsorption of sub-monolayer quantities [33]. Even the two–three orders of magnitude smaller magnetoelastic stress, which is the film analogon to magnetostriction of a bulk sample, has been measured successfully for films as thin as few atomic layers [8, 34].

The study of stress at surfaces and in ferromagnetic layers requires the use of an ultrahigh vacuum (UHV) chamber with the corresponding preparation tools and analyzing techniques, such as sample manipulator for cooling and heating, ion gun for sample cleaning, evaporators and leak valves to adsorb

various gases onto the substrate surface, Auger electron spectroscopy (AES) to check the elemental composition of the surface layer, low energy electron diffraction (LEED), and medium energy electron diffraction (MEED) for monitoring the sample structure. A key asset of the UHV chamber is the magnet system, which provides horizontal (0.4 T) and vertical (0.1 T) fields to perform magneto-optical Kerr-effect (MOKE) and magnetoelastic stress measurements in situ.

Figure 4 shows a simplified sketch of the UHV chamber that we designed in Halle to perform combined stress and magnetic measurements on surfaces and atomic layers. The incorporation of a magnet is mandatory to study magnetic properties of atomic layers in situ. An example for magnetization-induced stress measurements is given in the section on magnetoelastic stress, where the application of the cantilever curvature technique is described to measure magnetoelastic coupling coefficients of ferromagnetic layers.

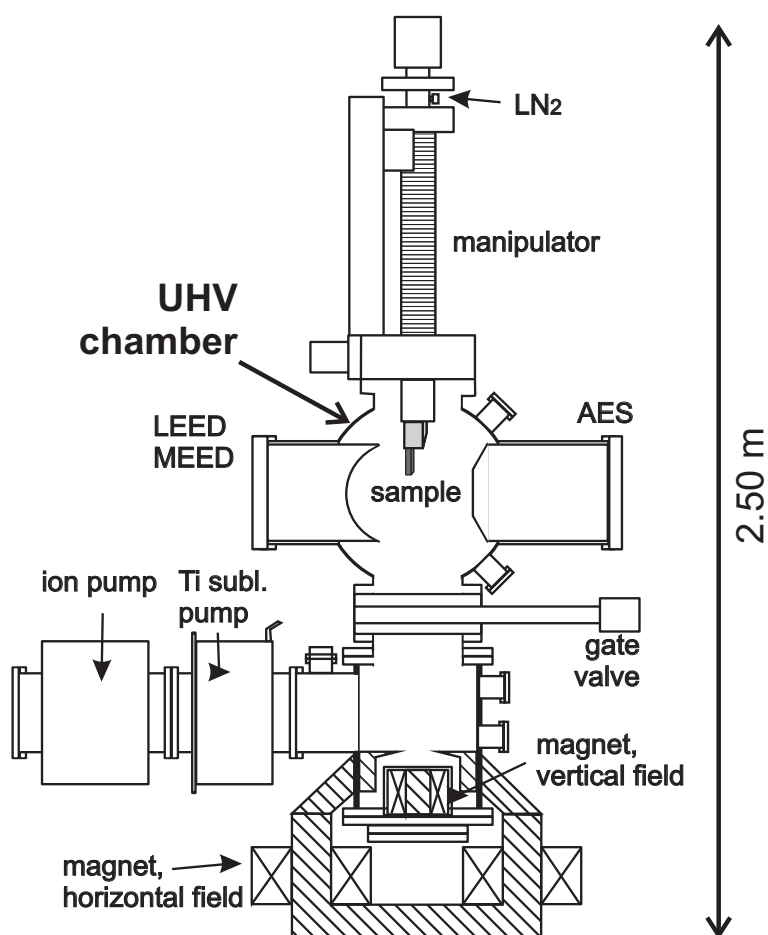


Figure 4. Sketch of the UHV chamber for in situ stress and magnetic studies. The sample can be lowered with the manipulator from the upper preparation level (LEED, MEED, AES) to the lower magnet level. At both levels optical deflection measurements as shown in Fig. 3 are mounted for stress during growth and magnetization-induced stress measurements, respectively.

3 Surface reconstruction and surface stress

The reduced coordination of surface atoms due to the lack of bonding partners above the surface leads to a peculiar redistribution of electronic charge near the surface region. This change of the electronic structure near the surface as compared to the bulk region can give rise to a change of the structure of a solid near its surface. Familiar phenomena are the change of the layer spacing at layers close to the surface as compared to the layer spacing in the bulk of the sample. This so-called layer relaxation has been found experimentally for numerous metallic surfaces, and it has been demonstrated that the magnitude of the layer relaxation depends on the adsorbate coverage of the surface [35].

In addition to the change of the layer spacing, also the forces between atoms within the surface layer change, as compared to bulk. Whereas in bulk the stability criterion of the equilibrium structure of the atomic positions is the requirement of a vanishing force acting between atoms, intra-atomic forces do act in the surface layer. Experimental and theoretical studies suggest that in general a tensile surface stress acts in a clean metal surface [7, 36, 37]. This surface stress can be viewed as an attractive interaction between neighboring atoms within the surface layer.

Thus, any adsorption onto a surface is expected to change the surface stress, as new bonds are formed between surface atoms and adsorbates, which in turn will change also the forces acting in the surface layer. Indeed, adsorbate-induced surface stress changes have been measured for numerous examples with the cantilever bending technique [7, 12, 33].

A most interesting question in this respect is, whether the adsorbate-induced change of surface stress can even drive a surface reconstruction [7, 38]. First experiments on the C-induced clock reconstruction of Ni(001) suggest that this might be so [39]. Here we present another example where we studied the link between oxygen-induced surface stress change and surface reconstruction of Cu(001) [37].

The exposure of clean Cu(001) to an O₂ partial pressure of the order 10⁻⁶ mbar at 300 K leads to the formation of an ordered c(2 × 2)-O adsorbate structure. If however, the exposure to O₂ is performed at a higher temperature of 500 K, a surface reconstruction is observed, where every fourth atomic row of Cu is expelled from the surface, and this leads to the missing row ($\sqrt{2} \times 2\sqrt{2}$)R45° reconstructed surface structure, which is experimentally well established [37, 38, 40]. Figure 5 illustrates the two different surface structures which result from the adsorption of oxygen at 300 K, panel (a), and at 500 K, panel (b).

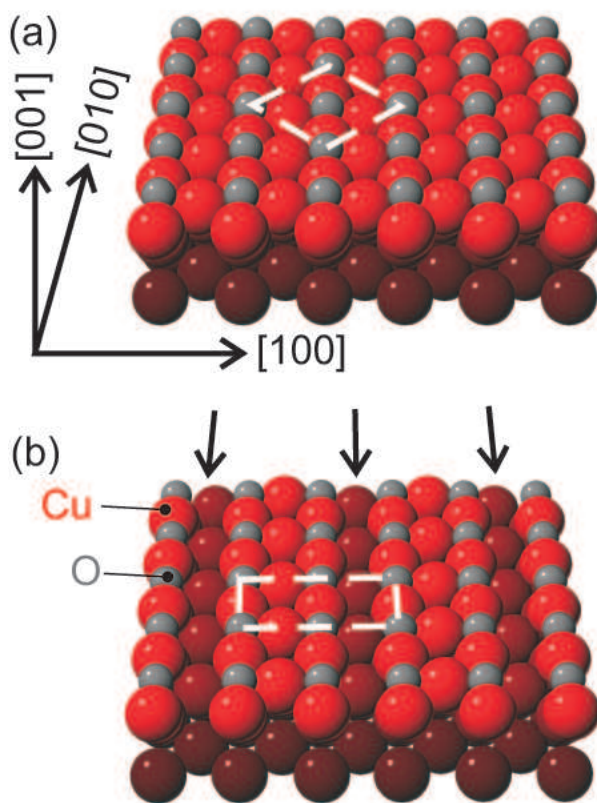


Figure 5. Oxygen-induced surface structure on Cu(001). (a) Oxygen atoms (grey) form a $c(2 \times 2)$ adsorbate structure on Cu(001) at 300 K. (b) Oxygen-adsorption at 500 K leads to the missing row $(\sqrt{2} \times 2\sqrt{2})R45^\circ$ reconstructed surface. The arrows indicate the missing rows of Cu surface atoms. Unit cells of the structures are indicated by the dashed white line.

We have performed measurements of the oxygen-induced change of surface stress of Cu(001) for a Cu substrate temperature of 300 K and 500 K, and the result is shown in Fig. 6 [37]. The low energy electron diffraction (LEED) images of Fig. 6 indicate the formation of the $c(2 \times 2)$ and missing row $(\sqrt{2} \times 2\sqrt{2})R45^\circ$ structure at 300 K and 500 K, respectively. The plots indicate that exposure to oxygen leads to a compressive stress change in both cases. The surface stress change saturates around -1 N/m for exposure at 300 K, and around -0.6 N/m at 500 K. The main conclusion of this measurement is that the stress change associated with the missing row reconstruction is smaller than the stress change due to the formation of the $c(2 \times 2)$ structure.

We need to appreciate this change of surface stress with respect to the absolute surface stress of this system. Absolute surface stress values are not accessible experimentally, only surface stress changes upon adsorption have been reliably determined. Therefore, density functional theory (DFT) slab calculations have been performed [37]. They give a tensile surface stress of $+1.89$ N/m for Cu(001), -1.18 N/m for the $c(2 \times 2)$ phase, and -0.67 N/m along the missing row, and $+0.4$ N/m perpendicular to the missing row of the missing row reconstructed phase [37]. These calculations indicate that the average surface stress of the missing row reconstructed phase of -0.14 N/m is lower in magnitude than that of the $c(2 \times 2)$ phase (-1.18 N/m). This result supports the view that the reduction of surface stress drives the missing row reconstruction.

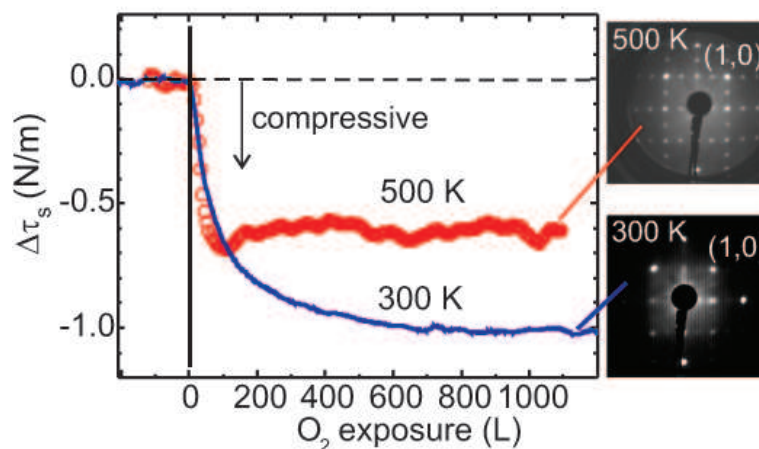


Figure 6. Surface stress change during exposure of Cu(001) to oxygen at 300 K (blue curve) and 500 K (red curve). The resulting LEED patterns ($E = 115$ eV) after oxygen exposure show the diffraction pattern of the missing row ($\sqrt{2} \times 2\sqrt{2}$)R45° structure (upper image) and the $c(2 \times 2)$ structure (lower image). Exposure to O₂ was performed at a partial pressure of order 10^{-6} mbar, and it is given in Langmuir (1 L = 10^{-6} torr s).

However, the experimentally determined surface stress change deviates noticeably from the calculated surface stress changes. We ascribe this to the important contribution of structural domains and stress relaxation at domain boundaries for both surface structures, which will lead to smaller experimental surface stress changes as compared to the calculated values.

This example illustrates that a proper assessment of the surface stress changes benefits largely from additional insight from *ab initio* based calculations. The following example of the surface stress change induced by surface alloying indicates that a decent agreement between experimental and calculated stress changes can be obtained for structurally more simple systems.

4 Surface stress and surface alloying

Numerous studies have shown that the adsorption of metal atoms on a metal surface may lead to a substitutional bonding site of the adsorbate [41]. The adsorbate atom may replace a surface atom of the substrate. If this intermixing is confined to the surface layer, which is the case for many systems, one obtains a surface alloy. These surface alloys may form for systems, which are immiscible in the bulk phase.

The study of surface alloys and the understanding of the driving forces behind surface alloy formation are of high interest, as the electronic, magnetic, and structural properties of a few atomic layer thin film are heavily influenced by the interface to the substrate [42–45].

Calculations suggest that the size mismatch between adsorbate atom and substrate atom is an important factor which drives a surface alloy formation. As pointed out by Tersoff, it is a remarkable observation that the same effect, atomic size mismatch, favors surface alloy formation, but suppresses

alloy formation in bulk phases [42].

Surface stress measurements offer additional insight into the mechanisms which drive surface alloy formation. We have investigated the formation of a prototype surface alloy, the $c(2 \times 2)$ -Mn/Cu(001) system [45], by combined surface stress and surface x-ray diffraction (SXRD) experiments. The combined experiments provide a comprehensive description of both stress and structure of the surface alloy layer [45].

The stress curve of Fig. 7 identifies two stress regimes. A compressive change of surface stress in proportion to the increasing Mn coverage up to the deposition of 0.5 ML Mn is observed in regime I. At this point a compressive stress change of -1.2 N/m is observed, and the LEED image identifies a pronounced $c(2 \times 2)$ structure. Further deposition of Mn leads to an almost negligible stress change in regime II, which levels off at -1.4 N/m after deposition of 2 ML Mn stress. The LEED images show an increased background intensity with increasing coverage.

Our stress data in connection with the detailed SXRD structural analysis indicate that the formation of the MnCu surface alloy is completed after deposition of 0.5 ML at 300 K. At this point, every second surface atom of Cu(001) is replaced with an Mn atom, and a $c(2 \times 2)$ surface structure results [45].

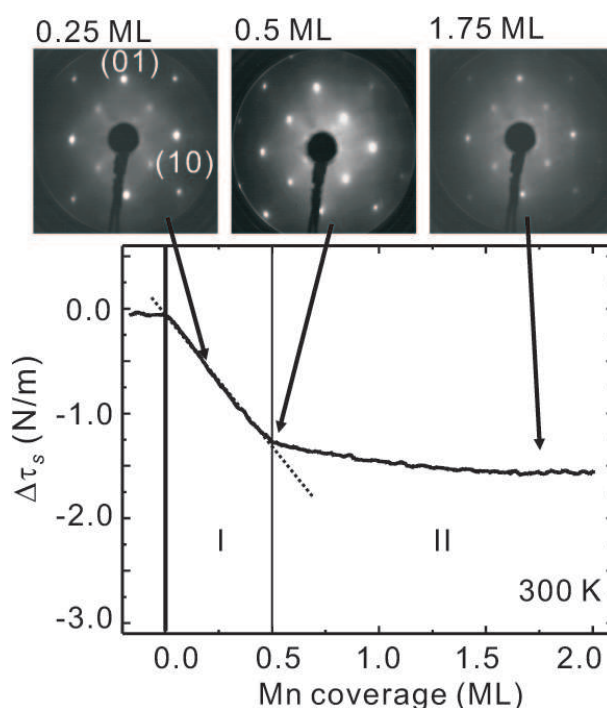


Figure 7. Surface stress change during the deposition of Mn on Cu(001) at 300 K. The top panels give LEED images ($E = 112$ eV), which were taken at the indicated Mn coverage. The surface stress $\Delta\tau_s$ changes in proportion to the Mn coverage in region I, as indicated by the dotted line. The Mn coverage is given in monolayer (1 ML = 1 Mn atom per Cu surface atom).

The magnitude of the measured stress change (-1.2 N/m) is a factor of two larger than what is expected based on the epitaxial misfit between MnCu and Cu(001). This result immediately points at

the reduction of tensile surface stress of Cu(001) upon surface alloy formation, which contributes to the stress measurement as a compressive stress.

This assertion is corroborated by recent DFT calculations [46], which find a surface stress change upon MnCu surface alloy formation of -1.52 N/m, in fair agreement with our experimental value of -1.2 N/m. The magnitude of the stress change renders the Cu surface almost free of surface stress. Thus, our stress measurements in conjunction with theory [46] indicate that the reduction of surface stress of Cu might play a crucial role for this surface alloy formation.

One important implication of this finding is that surface stress measurements offer quantitative data, which may serve as a comparison for theory. This combination between experiment and theory offers deeper insight into the underlying physics by considering also forces between atoms, an aspect which has not been studied in detail before.

5 Film stress and film structure

Cantilever stress measurements have a long tradition for the measurement of film stress. Very different topics including stress in amorphous films, stress in epitaxial films, stress relaxation due to misfit formation, structural- and morphology-induced stress change have been investigated. Several reviews and data compilations [1–12] and publications [13–19] provide further insight.

A strength of stress measurements is that quantitative values for film stress are obtained directly from the analysis of the substrate curvature. This allows to compare the measured stress with the calculated stress, where the calculation is based on model assumptions regarding the film structure. Very often pseudomorphically strained epitaxial films are studied. In this case, the epitaxial misfit gives rise to a film strain, which induces the film stress. Our measurements on few monolayer thin films do indeed confirm, that bulk reference states are appropriate to derive film stress from strain for films thicker than 1–2 monolayers [43, 47–49].

For thinner films, surface stress effects might dominate the stress behavior, rendering the concept of film strain irrelevant for the resulting stress. Examples include the sub-monolayer stress of Fe and Ni on W(110), where even a stress of opposite sign as compared to the expected stress due to film strain is measured for a film coverage below 0.5 layers [14, 26].

Here, we present in Fig. 8 stress measurements during the growth of epitaxial Fe films on Ir(001), where scanning tunneling microscopy (STM) and a quantitative structural analysis by LEED indicate almost perfect layer-by-layer growth with a constant in-plane film strain from 0 to 10 ML Fe coverage [50]. In contrast to the constant in-plane strain from 0–10 ML, the stress curve shows a variation of its slope around 2 ML. The positive slope of the curve indicates a tensile film stress of $+6$ GPa from 1–2 ML, and it shows a negative slope corresponding to a compressive film stress of -10 GPa from 2–10 ML.

The initial negative slope of the stress curve up to 0.5 ML is ascribed to Fe-induced reduction of surface stress of Ir. The deviation of the stress curve from its constant slope above 10 ML indicates stress relaxation due to the formation of misfit dislocations, which begin to form around 10 ML, and they also give rise to a characteristic change of the diffraction pattern in LEED.

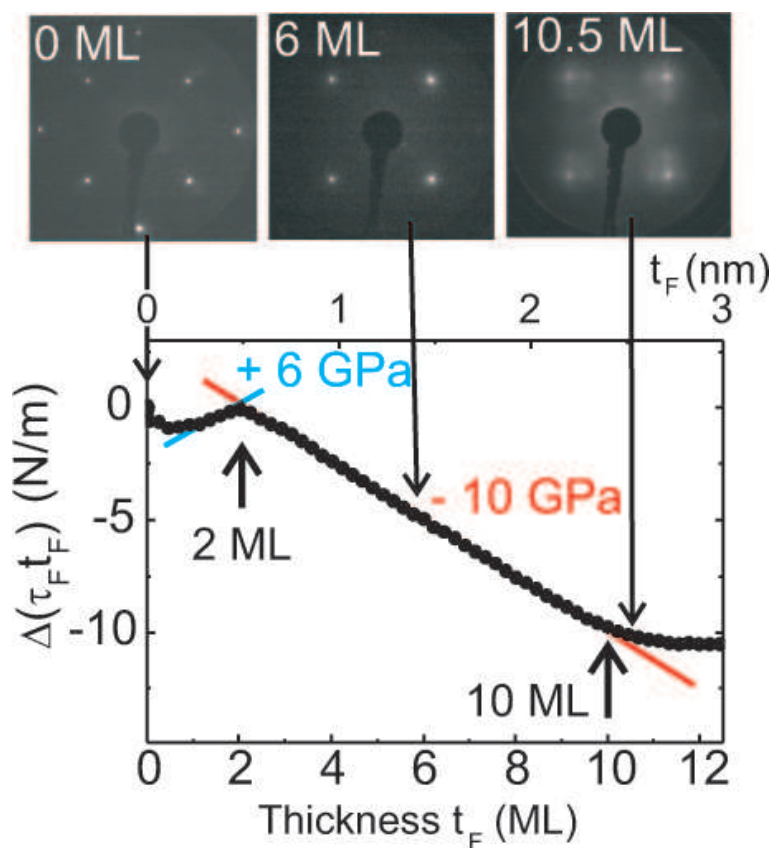


Figure 8. Film stress during deposition of Fe on Ir(001) at 300 K. The top panels show LEED images ($E = 98$ eV), taken at the indicated thickness. Kinks of the stress curve are observed around 2 ML and 10 ML, indicating the end of growth of a fct-precursor and of epitaxially strained bct-Fe, respectively.

The top panel of Fig. 8 shows LEED images which were taken at the indicated film thickness. Already a qualitative inspection reveals the end of pseudomorphic growth at 10.5 ML. An area of enhanced diffuse intensity with weak extra spots develops towards the center of the LEED screen around the spots indicative of the 1×1 structure [50], and this ascribed to the onset of misfit dislocation formation at 10.5 ML.

Note the amazingly high magnitude of the film stress of -10 GPa from 2–10 ML. This strikingly demonstrates that film stress in a magnitude well beyond the yield stress of high strength bulk materials is accessible in ultrathin films, and this renders the investigation of the correlation between stress, structure and magnetism of strained films so interesting [8]. The magnitude of stress is quantitatively ascribed to the compressive epitaxial misfit of -5.6% between bcc-Fe and Ir(001) [50].

The initial tensile film stress cannot be ascribed to the misfit between bcc-Fe and Ir. Rather our stress measurements, in connection with a detailed structural analysis by LEED, where also the vertical layer spacings of the Fe film are analyzed, suggests that the first two layers of Fe grow as a fct-precursor. A tensile epitaxial misfit is expected for fcc-Fe growth on Ir(001), and this explains qualitatively the tensile film stress. Subsequent Fe depositions leads to the growth of bct-Fe on top of this precursor. A detailed discussion of this scenario is given in reference [50].

This example demonstrates that stress measurements are a powerful tool to observe subtle structural transitions in atomic layers, even in cases where no change of the in-plane strain is observed. The combination of stress measurements with structural investigation offers a comprehensive understanding of structural transitions.

6 Magnetoelastic stress of ferromagnetic layers

The magnetic anisotropy of ferromagnetic layers determines the orientation of the easy and hard magnetization directions, and it can also have an important impact on the magnitude of the coercive field [51, 52]. A lot of experimental and theoretical work has been devoted to the understanding of the principles which govern the magnetic anisotropy [8, 34, 53–55]. These studies suggest lattice strain as an important factor, which often determines the magnetic anisotropy of atomic layers.

The coupling between lattice strain and magnetic anisotropy is given by the magnetoelastic coupling, which gives rise to magnetostriction, i.e. the change of length of a bulk sample upon magnetization [51, 57]. Ferromagnetic films are usually bonded to a substrate, and the films are not free to strain upon magnetization. Here, the lattice strain, as given e.g. by the epitaxial misfit between film and substrate, induces a magnetic anisotropy, which determines in many cases the easy magnetization direction of the film. Thus, a detailed understanding of the magnetoelastic coupling in films is mandatory to understand and tailor their magnetic properties.

In contrast to bulk samples, where the magnetization leads to a magnetostrictive strain, the magnetization of a film-substrate composite leads to a magnetoelastic stress. This stress is typically 2–3 orders of magnitude smaller than the epitaxial misfit stress discussed above, which is of the order of GPa per one percent misfit. In spite of this minute magnetoelastic stress, stress measurements by the cantilever curvature technique provide quantitative and accurate measurements of the underlying magnetoelastic coupling coefficients B_i [8, 20, 58].

Magnetoelastic stress measurements are performed by monitoring the change of a curvature of the film-substrate composite upon a reorientation of the film magnetization along two orthogonal directions. Depending on the crystalline orientation, different magnetoelastic coupling coefficients are determined [59, 60]. Figure 9 illustrates the magnetization directions along a cantilever sample, and it shows the magnetoelastic stress curve of 8 ML Fe on Ir(001) [56]. Switching the magnetization direction along these directions gives access to $B_1 = \tau^{100} - \tau^{010} = \Delta\tau$. The plot of Fig. 9 reveals that the magnetoelastic stress (red curve) changes upon a reorientation of the magnetization direction from along the sample length to along the sample width. Simultaneously taken magneto-optical Kerr-effect (MOKE) [61] measurements (blue curve) verify that the magnetization direction switched in the described manner. A magnetoelastic stress $\Delta\tau = 0.01$ N/m is measured. Note that this is roughly 3 orders of magnitude smaller than the film stress measured for 10 ML Fe on Ir(001), shown in Fig. 8.

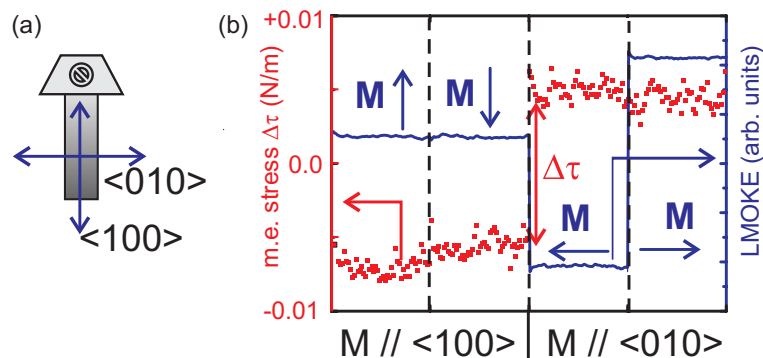


Figure 9. (a) Sketch of the magnetization directions for the magnetoelastic stress measurement of (b). The red curve shows the magnetoelastic stress change upon a magnetization reorientation in-plane (indicated in (a)), which is monitored also by longitudinal MOKE measurements (LMOKE, blue curve) [56].

The magnetoelastic stress change of 0.01 N/m corresponds to $B_1 = -10 \text{ MJ/m}^{-3}$ [56]. This value is a factor of almost 3 larger than the respective bulk value of -3.4 MJ/m^{-3} . Numerous detailed studies of the magnetoelastic coupling of strained epitaxial films reveal, that a deviation between the B_i of a film and that of the respective bulk material is the rule. This result has important implications. It indicates, that bulk values of B_i do not give an appropriate description of magnetoelastic coupling in films [8].

Rather, the results from combined film stress and magnetoelastic stress measurements suggest that film strain is a decisive factor which drives the deviation of B_i from its bulk value [8, 56, 62]. This impact of film strain on the magnetoelastic coupling has been also identified in state of the art calculations of magnetoelastic coupling in elements [63–66] and alloys [67]. However, the agreement between theory and experiment for the magnetoelastic coupling of elements is qualitative at best presently. This calls for more experiments and theoretical efforts in this field to gain a deeper understanding of the electronic origin of the influence of strain on the magnetic anisotropy.

7 Conclusion

We have demonstrated that highly accurate and sensitive data on stress and magnetoelastic coupling are accessible in cantilever experiments. These measurements elucidate the correlation between stress and surface alloying, reconstruction, structural transitions, and magnetic properties of surfaces and in atomic layers.

Thus, stress measurements contribute to an improved understanding of fundamental aspects of surface science by providing accurate quantitative values for forces acting within a surface. The consideration of forces at surfaces has been neglected a bit in experiments and theory so far. Related work has attracted much less attention as compared to e.g. investigations of structural and electronic aspects. Ongoing efforts from experiment and theory are therefore called for to advance in the understanding of the correlation between stress, structure and magnetic anisotropy at surfaces and in atomic layers at a fundamental level. Cantilever measurements are an appropriate tool to contribute to this effort.

Acknowledgements

The authors thankfully acknowledge previous coworkers and guests who contributed to various aspects of the experiments described: Axel Enders, Thomas Gutjahr-Löser, Thomas Höpfl, Safia Ouazi, Wei Pan, Mahesh Rajappan, Sergei Zharkov Hellmut Höche, and Heike Menge for the skillful preparation of thin single crystalline substrates.

References

1. Abermann, R. Measurement of the intrinsic stress in thin metal films. *Vacuum* **1990**, *41*, 1279–1282.
2. Koch, R.; Leonhard, H.; Thurner, G.; Abermann, R. A UHV compatible thin film stress measuring apparatus based on the cantilver beam principle. *Rev. Sci. Instrum.* **1990**, *61*, 3859–3862.
3. Bain, J. A.; Chyung, L. J.; Brennan, S.; Clemens, B. M. Elastic strains and coherency stresses in Mo/Ni multilayers. *Phys. Rev. B* **1991**, *44*, 1184–1192.
4. Koch, R. The intrinsic stress of polycrystalline and epitaxial thin metal films. *J. Phys.: Condens. Matter* **1994**, *6*, 9519–9550.
5. Spaepen, F.; Shull, A. L. Mechanical properties of thin films and multilayers. *Current Opinion in Solid State and Materials Science* **1996**, *1*, 679–683.
6. Koch, R. *Intrinsic stress of epitaxial thin films and surface layers*, volume 8 of *The chemical physics of solid surfaces*. Elsevier, Amsterdam, **1997**.
7. Ibach, H. The role of surface stress in reconstruction, epitaxial growth and stabilization of mesoscopic structures. *Surf. Sci. Rep.* **1997**, *29*, 193–264.
8. Sander, D. The correlation between mechanical stress and magnetic anisotropy in ultrathin films. *Rep. Prog. Phys.* **1999**, *62*, 809–858.
9. Nix, W.; Clemens, B. Crystallite coalescences: a mechanism for intrinsic stress in thin films. *J. Mater. Res.* **1999**, *14*, 3467–3473.
10. Spaepen, F. Interfaces and stresses in thin films. *Acta Materialia* **2000**, *48*, 31–42.
11. Sander, D. *Stress and Strain in Epitaxy*, chapter Stress measurements of atomic layers and at surfaces, pages 221–242. Elsevier, **2002**.
12. Sander, D.; Ibach, H. *Surface free energy and surface stress*, chapter 4.4, pages 4.4–1 – 4.4–49. Landolt-Börnstein, Numerical Data and Functional Relationships in Science and Technology, New Series, Group III: Condensed Matter, Volume 42, A 2. Springer, Berlin, **2002**.
13. Mayr, S.; Samwer, K. Model for intrinsic stress formation in amorphous thin films. *Phys. Rev. Lett.* **2001**, *87*, 036105–1–036105–4.
14. Meyerheim, H.; Sander, D.; Popescu, R.; Kirschner, J.; Robach, O.; Ferrer, S.; Steadman, P. Ni-induced giant stress and surface relaxation in W(110). *Phys. Rev. B* **2003**, *67*, 155422.
15. Okumu, J.; Koerfer, F.; Salinga, C.; Wuttig, M. In situ measurements of thickness changes and mechanical stress upon gasochromic switching of thin moo[sub x] films. *Journal of Applied Physics* **2004**, *95*(12), 7632–7636.
16. Horn-von Hoegen, M.; Müller, B. H.; Grabosch, T.; Kury, P. Strain relief during Ge hut cluster formation on Si(001) studied by high-resolution leed and surface-stress-induced optical deflection.

- Phys. Rev. B* **2004**, *70*, 235313.
17. Kury, P.; Grabosch, T.; von Hoegen, M. H. SSIOD: The next generation. *Review of Scientific Instruments* **2005**, *76*(2), 023903.
 18. Drese, R. J.; Wuttig, M. In situ stress measurements in zirconium and zirconium oxide films prepared by direct current sputtering. *Journal of Applied Physics* **2006**, *99*(12), 123517.
 19. Vecchio, A. L. D.; Spaepen, F. The effect of deposition rate on the intrinsic stress in copper and silver thin films. *Journal of Applied Physics* **2007**, *101*(6), 063518.
 20. Weber, M.; Koch, R.; Rieder, K. UHV cantilever beam technique for quantitative measurements of magnetization, magnetostriction, and intrinsic stress of ultrathin films. *Phys. Rev. Lett.* **1994**, *73*, 1166–1169.
 21. Rossel, C.; Willemin, M.; Gasser, A.; Bothuizen, H.; Meijer, G.; Keller, H. Torsion cantilever as magnetic torque sensor. *Rev. Sci. Instrum.* **1998**, *69*, 3199–3203.
 22. Höpfl, T.; Sander, D.; Höche, H.; Kirschner, J. Ultrahigh vacuum cantilever magnetometry with standard size single crystal substrates. *Rev. Sci. Instr.* **2001**, *72*, 1495–1501.
 23. Gao, L.; Feng, D. Q.; Yuan, L.; Yokota, T.; Sabirianov, R.; Liou, S. H.; Chabot, M. D.; Porpora, D.; Moreland, J. A study of magnetic interactions of Ni₈₀Fe₂₀ arrays using ultrasensitive microcantilever torque magnetometry. *J. Appl. Phys.* **2004**, *95*, 7010–7012.
 24. Stoney, G. The tension of metallic films deposited by electrolysis. *Proc. R. Soc. London A* **1909**, *82*, 172–175.
 25. Dahmen, K.; Lehwald, S.; Ibach, H. Bending of crystalline plates under the influence of surface stress. *Surf. Sci.* **2000**, *446*, 161–173.
 26. Sander, D.; Enders, A.; Kirschner, J. Anisotropic surface stress on W(110). *Europhys. Lett.* **1999**, *45*, 208–214.
 27. Nye, J. F. *Physical Properties of Crystals*. Oxford University Press, Oxford, **1985**.
 28. Hearmon, R. F. S. *The elastic constants of non-piezoelectric crystals*, volume 2 of *Landolt-Börnstein Numerical Data and Functional Relationships in Science and Technology Group III*. Springer-Verlag, Berlin, **1969**.
 29. Hearmon, R. F. S. *The elastic constants of crystals and other anisotropic materials*, volume 18 of *Landolt-Börnstein Numerical Data and Functional Relationships in Science and Technology Group III*. Springer-Verlag, Berlin, **1984**.
 30. Brantley, W. A. Calculated elastic constants for stress problems associated with semiconductor devices. *J. Appl. Phys.* **1973**, *44*, 534–535.
 31. He, L.; Lim, C. On the bending of unconstrained thin crystalline plates caused by the change in surface stress. *Surf. Sci.* **2001**, *478*, 203–210.
 32. k-space Associates, Inc., <http://www.k-space.com/>; LAFOUDA Solutions, <http://www.lafouda.com/>.
 33. Sander, D. Surface stress: implications and measurements. *Curr. Opinion Solid St. Mat. Sci.* **2003**, *1*, 51–57.
 34. Sander, D. The magnetic anisotropy and spin reorientation of nanostructures and nanoscale films. *J. Phys.: Condens. Matter* **2004**, *16*, R603–R636.
 35. Sander, D.; Pand, W.; Ouazi, S.; Kirschner, J.; Meyer, W.; Krause, M.; Müller, S.; Hammer, L.;

- Heinz, K. Reversible H-induced switching of the magnetic easy axis in Ni/Cu(001) thin films. *Phys. Rev. Lett.* **2004**, *93*, 247203.
36. Feibelman, P. First-principles calculations of stress induced by gas adsorption on Pt(111). *Phys. Rev. B* **1997**, *56*, 2175–2182.
37. Harrison, M.; Woodruff, D.; Robinson, J.; Sander, D.; Pan, W.; Kirschner, J. Adsorbate-induced surface reconstruction and surface stress changes in Cu(100)/O: experiment and theory. *Phys. Rev. B* **2006**, *74*, 165402–1.
38. Wuttig, M.; Franchy, R.; Ibach, H. Oxygen on Cu(100) - a case of adsorbate-induced reconstruction. *Surf. Science* **1989**, *213*, 103–136.
39. Sander, D.; Linke, U.; Ibach, H. Adsorbate-induced surface stress: sulfur, oxygen and carbon on Ni(100). *Surf. Sci.* **1992**, *272*, 318–325.
40. Robinson, I. K.; Vlieg, E.; Ferrer, S. Oxygen-induced missing-row reconstruction of Cu(001) and Cu(001)-vicinal surfaces. *Phys. Rev. B* **1990**, *42*, 6954–6962.
41. Woodruff, D., editor. *The chemical physics of solid surfaces*, volume 10. Elsevier, Amsterdam, **2002**.
42. Tersoff, J. Surface-confined alloy formation in immiscible systems. *Phys. Rev. Lett.* **1995**, *74*, 434–437.
43. Pan, W.; Sander, D.; Lin, M.-T.; Kirschner, J. Stress oscillations and surface alloy formation during the growth of FeMn on Cu(001). *Phys. Rev. B* **2003**, *68*(22), 224419.
44. Longo, R. C.; Stepanyuk, V. S.; Hergert, W.; Vega, A.; Gallego, L. J.; Kirschner, J. Interface intermixing in metal heteroepitaxy on the atomic scale. *Phys. Rev. B* **2004**, *69*, 073406.
45. Pan, W.; Popescu, R.; Meyerheim, H.; Sander, D.; Robach, O.; Ferrer, S.; Lin, M.-T.; Kirschner, J. Stress and structure of c(2x2) and p2gg(4x2) Mn/Cu(001) surface alloys. *Phys. Rev. B* **2005**, *174439*, 174439.
46. Harrison, M.; Woodruff, D.; Robinson, J. Alloying-induced surface stress change in Cu(100)c(2x2)-Mn. *Phys. Rev. B* **2005**, *72*, 113408–1–113408–3.
47. Gutjahr-Löser, T. *Magnetoelastische Kopplung in oligatomaren Filmen*. PhD thesis, Martin-Luther Universität Halle-Wittenberg, Mathematisch-Naturwissenschaftlich-Technische Fakultät, **1999**.
48. Sander, D.; Ouazi, S.; Stepanyuk, V.; Bazhanov, D.; Kirschner, J. Stress oscillations in a growing metal film. *Surf. Sci.* **2002**, *512*, 281–286.
49. Mahesh, R.; Sander, D.; Zharkov, S.; Kirschner, J. Stress and growth of Ag monolayers on a Fe(100) whisker. *Phys. Rev. B* **2003**, *68*, 045416.
50. Martin, V.; Meyer, W.; Giovanardi, C.; Hammer, L.; Heinz, K.; Tian, Z.; Sander, D.; Kirschner, J. Pseudomorphic growth of Fe monolayers on Ir(001)-(1 x 1): From a fct precursor to a bct film. *Phys. Rev. B* **2007**, *76*, 205418.
51. Kittel, C. Physical theory of ferromagnetic domains. *Rev. Mod. Phys.* **1949**, *21*, 541–583.
52. Sander, D.; Skomski, R.; Schmidhals, C.; Enders, A.; Kirschner, J. Film stress and domain wall pinning in sesquilayer iron films. *Phys. Rev. Lett.* **1996**, *77*, 2566–2569.
53. Gradmann, U. *Surfaces, interfaces, and ultrathin films*, volume 19 of *Landolt-Börnstein Numerical Data and Functional Relationships in Science and Technology Group III*. Springer-Verlag, Berlin, 1988.

54. Uiberacker, C.; Zabloudil, J.; Weinberger, P.; Szunyogh, L.; Sommers, C. Lattice relaxation driven reorientation transition in Ni_n/Cu(100). *Phys. Rev. Lett.* **1999**, *82*, 1289–1292.
55. Maca, F.; Shick, A.; Redinger, J.; Podloucky, R.; Weinberger, P. The influence of hydrogen adsorption on magnetic properties of Ni/Cu(001) surface. *Czech. J. Phys.* **2003**, *53*, 33–39.
56. Zhen, T. Max Planck Institute of Microstructure Physics, Halle, Germany (2008).
57. du Trémolet de Lacheisserie, E. *Magnetostriction*. CRC-Press, Boca Raton, **1993**.
58. du Trémolet de Lacheisserie, E.; Peuzin, J. Magnetostriction and internal stresses in thin films: the cantilever method revisited. *J. Magn. Magn. Mater.* **1994**, *136*, 189–196.
59. Dahmen, K.; Ibach, H.; Sander, D. A finite element analysis of the bending of crystalline plates due to anisotropic surface and film stress applied to magnetoelasticity. *J. Magn. Magn. Mater.* **2001**, *231*, 74–84.
60. Sander, D.; Kirschner, J. Cantilever stress measurements of ferromagnetic monolayers. *Appl. Phys. A* **2007**, *87*, 419–425.
61. Bader, S. SMOKE. *J. Magn. Magn. Mat.* **1991**, *100*, 440–454.
62. Koch, R.; Weber, M.; Rieder, K. Magnetoelastic coupling of Fe at high stress investigated by means of epitaxial Fe(001) films. *J. Magn. Magn. Mater.* **1996**, *159*, L11–L16.
63. Fähnle, M.; Komelj, M.; Wu, R.; Guo, G. Magnetoelasticity of Fe: possible failure of ab initio electron theory with the local-spin-density approximation and with the generalized-gradient approximation. *Phys. Rev. B* **2002**, *65*, 144436–1–144436–5.
64. Komelj, M.; Fähnle, M. Determination of the complete set of second-order magnetoelastic coupling constants on epitaxial films. *Phys. Rev. B* **2002**, *65*, 212410–1–212410–4.
65. Burkert, T.; Nordström, L.; Eriksson, O.; Heinonen, O. Giant magnetic anisotropy in tetragonal FeCo alloys. *Phys. Rev. Lett.* **2004**, *93*, 027203.
66. Komelj, M.; Fähnle, M. Nonlinear magnetoelastic behavior of the bcc phases of Co and Ni: Importance of third-order contributions for bcc Ni. *Phys. Rev. B* **2006**, *73*, 012404.
67. Burkert, T.; Eriksson, O.; James, P.; Simak, S.; Johansson, B.; Nordström, L. Calculation of uniaxial magnetic anisotropy energy of tetragonal and trigonal Fe, Co, Ni. *Phys. Rev. B* **2004**, *69*, 104426–1–104426–7.